Journal of Zhejiang University-SCIENCE B (Biomedicine & Biotechnology) in press
www.jzus.zju.edu.cn; www.springer.com/journal/11585
E-mail: jzus_b@zju.edu.cn

Research Article

https://doi.org/10.1631/jzus.B2400192

CXCL16 promotes proliferation of head and neck squamous cell carcinoma by regulating GPX1-mediated antioxidant levels

Ru HE[1*], Hongyi JIANG[1,6*], Chengchi ZHANG[2], Yuan CHEN[3], Wenshun LIU[4], Xinyue DENG[1,6], Xiaozheng ZHU[1,6], Yunye LIU[1], Chuanming ZHENG[1,6], Yining ZHANG[5], Chengying SHAO[5], Yanting DUAN[1,6]✉, Jiajie XU[1,6]✉

[1]*Otolaryngology & Head and Neck Center, Cancer Center, Department of Head and Neck Surgery, Zhejiang Provincial People's Hospital, Affiliated People's Hospital, Hangzhou Medical College, Hangzhou 310014, China*
[2]*Zhejiang University of Technology, Hangzhou 310014, China*
[3]*Cancer Center, Department of Pathology, Zhejiang Provincial People's Hospital (Affiliated People's Hospital), Hangzhou Medical College, Hangzhou 310014, China*
[4]*Jinzhou Medical University, Department of Postgraduate Education, Jinzhou 121000, China*
[5]*Second Clinical Medical College, Zhejiang Chinese Medical University, Hangzhou 310053, China*
[6]*Key Laboratory of Endocrine Gland Diseases of Zhejiang Province, Hangzhou 310014, China*

Unedited

Abstract: Numerous studies have demonstrated that high expression of the CXC motif chemokine ligand 16 (CXCL16) in cancer correlates with poor prognosis, as well as tumor cell proliferation, migration and invasion. While CXCL16 can serve as a tumor biomarker, the underlying mechanism in modulating head and neck squamous carcinoma (HNSCC) remains unclear. In this study, we aimed to investigate CXCL16 expression in head and neck squamous carcinoma and uncover the potential underlying mechanism. We determined the high expression of CXCL16 in The Cancer Genome Atlas (TCGA) database, tissue samples from patients with head and neck squamous cell carcinoma at our central hospital and from HNSCC cell lines. The results showed that CXCL16 knockdown inhibited the proliferation, migration and invasion of HNSCC cells. Mechanistically, transcriptome sequencing revealed that CXCL16 may affect HNSCC cell growth by regulating the antioxidant pathway of glutathione peroxidase 1 (GPX1). ROS levels were elevated in si-CXCL16 cells, which may contribute to the inhibition of cell proliferation, migration and invasion. Moreover, treatment of cells with the GPX1 inhibitor eldecalcitol (ED-71) revealed that HNSCC cell growth was significantly inhibited in the synergistic group of si-CXCL16 and GPX1 inhibitor compared to the si-CXCL16 group. In conclusion, CXCL16 contributed to the development of HNSCC cells by modulating the GPX1-mediated antioxidant pathway. Thus, targeting cellular CXCL16 expression seems a promising strategy for treating head and neck squamous cell carcinoma.

Key words: Antioxidant pathway; CXC motif chemokine ligand 16 (CXCL16); Glutathione peroxidase 1 (GPX1); Head and neck squamous cell carcinoma

✉ Yanting DUAN, dyt19880818@163.com
Jiajie XU, xujiajie@hmc.edu.cn
* The two authors contributed equally to this work
Ru HE, https://orcid.org/0000-0002-9712-3386,
Hongyi JIANG, https://orcid.org/0009-0005-1696-9160

Received Apr. 15, 2024; Revision accepted July 29, 2024;
Crosschecked xxx. xx, 20xx; Published online xxx. xx, 20xx

© Zhejiang University Press 2024

1 Introduction

Head and neck squamous cell carcinoma (HNSCC), originating from the squamous mucosa of the upper aerodigestive tract, including the nasal cavity, nasopharynx, larynx, hypopharynx, and oropharynx, is ranked sixth among cancer-related deaths worldwide, with over 350,000 new cases and 170,000 deaths reported annually (Fan et al., 2011; Bray et al., 2018; Siegel et al., 2020). While diagnosis and multimodal treatment have recently shown rapid advancement, the 5-year survival rates remain low because of the complex anatomy of the head and neck (Brockstein et al., 2004). Cancer immunotherapy has gained widespread use in clinical settings in recent years, leading to significant changes in HNSCC treatment. For example, checkpoint inhibitors targeting PD-1, PD-L1, and CTLA-4, either alone or combined with radiotherapy or chemotherapy, as well as novel approaches based on cytokines or overt T-cell therapy are being investigated in clinical trials (Mei et al., 2020; Moreira et al., 2021; Hsieh et al., 2022). Although these immunotherapies have demonstrated significant benefits in some patients with advanced HNSCC, because of tumor heterogeneity, the effect of immunosuppressants remains inferior compared to the initial expectations. The objective remission rate is limited, with fewer than 20% of patients experiencing clinical benefit and most facing poor prognosis (Siu et al., 2019; Saddawi-Konefka et al., 2022). Therefore, there is an urgent need for effective biomarkers to predict the progression of HNSCC, thus enabling accurate and efficient disease status assessment to improve prognosis and reduce mortality rates.

Chemokines, a group of factors with chemotactic properties, control the migration and localization of immune cells, playing an essential role in the movement of all immune cells (Griffith et al., 2014). CXC motif chemokine ligand 16 (CXCL16) is a CXC-soluble chemokine with its gene located on chromosome 17p13, a separate locus distinct from other known chemokines (Matloubian et al., 2000; Izquierdo et al., 2014). Studies have shown that CXCL16 factors function in two primary forms: membrane-bound molecules and soluble chemokines (Abel et al., 2004). It has been found that soluble CXCL16 can activate the expression of transmembrane CXCL16 through homodimerization and enhance the proliferation and anti-apoptotsis of tumor cells by the phosphorylation of intracellular kinases (Hattermann et al., 2016).

Among the chemokine receptors, it was found that the specific receptor for CXCL16 is CXCR6, that is potentially involved in metabolic disorders, inflammatory responses, and T-cell migration and recruitment in vivo through the CXCR6-CXCL16 signaling axis (Matloubian et al., 2000; Collado et al., 2018; Karaki et al., 2021). Therefore, many researchers have investigated the role of this signaling axis in cancer. It was shown to have an intimate relationship with tumor progression and poor prognosis, as it promoted the growth, migration, and invasive ability of microglioma, thyroid cancer, lung cancer and gastric cancer cells, as well as epithelial-mesenchymal transition (EMT) pathway transformation (Hu et al., 2014; Cho et al., 2016; Lepore et al., 2018; Han et al., 2021). Several studies have reported that high CXCL16 expression in tumors contributes to tumor growth and invasion in the microenvironment by polarizing macrophages toward M2 and increasing angiogenesis (Kim et al., 2019). Additionally, in pancreatic ductal adenocarcinoma, the deletion of growth inhibitory receptor subtype 2 (SST2) expression activates PI3K, leading to NF-κB and oncogenic KRAS signaling activation, increased CXCL16 expression, and pancreatic tumor formation (Chalabi-Dchar et al., 2015). The role of CXCL16 is crucial in the onset and progression of cancer; however, the molecular mechanism of tumor cell metastasis promotion needs to be explored further.

Glutathione peroxidase 1 (GPX1) is an essential antioxidant enzyme in cells, capable of oxidizing glutathione (GSH) to its disulfide form and maintaining cellular redox balance by regulating intracellular reactive oxygen species (ROS) levels (Zhao et al., 2022). It has been found that HNSCC patients with a higher oxidative stress GSSG/GSH ratio have a higher risk of local tumor recurrence rate after treatment (Dequanter et al., 2017). Therefore, studying the mechanism related to oxidative stress in HNSCC cells can provide a basis for enriching the prognosis of HNSCC patients. Eldecalcitol (ED-71), a novel active vitamin D analog with anti-osteoporotic properties, could inhibit GPX1 expression and suppress oral cancer progression (Liu et al., 2022; Lu et al., 2023). On the other hand, chemokines associated with GPX1 in HNSCC have been rarely reported.

unedited

In our study, knockdown of CXCL16 expression in HNSCC cells significantly downregulated the expression level of GPX1 and inhibited the antioxidant capacity of HNSCC cells, thereby suppressing their proliferation and metastatic ability. Our study provides an important basis for using CXCL16 as a candidate molecule for diagnosing or treating HNSCC.

2 Materials and methods

2.1 Patients and follow-up

The selected cohort comprised 11 patients with oral squamous cell carcinoma who underwent surgery between 2022 and 2023. All patients were informed of sample collection and use. Tissue samples were taken and used according to the protocols approved by the Human Research Ethics Committee of Zhejiang Provincial People's Hospital. This study was conducted in accordance with the Declaration of Helsinki and national and international guidelines (Acceptance Number: QT2024066). A total of 559 patients with HNSCC were included in The Cancer Genome Atlas (TCGA) database.

2.2 Immunohistochemical assays and analysis

After fixation, dehydration, wax dipping, and paraffin embedding, the tissues were cut into 3 μm thick sections and adhered to slides. Endogenous peroxides and non-specific proteins were blocked with 3% hydrogen peroxide. Tissue sections were treated overnight with primary antibodies CXCL16 (AF976, Bio-Techne) and CXCR6 (AP73581, Abcepta) at 4℃. The next day, sections were washed three times and stained with secondary antibodies for 30 min at room temperature. Subsequently, the tissue sections were stained with diaminobenzidine for 3 min and nuclei were counterstained with hematoxylin for 1 min at room temperature. The CXCL16 staining scoring criteria were as follows: Intensity of staining: 0–no detectable staining, 1–light yellow, 2–medium yellow, 3–deep yellow, percentage of staining: 1 (≤ 10%), 2 (10-50%), 3 (50-80%), or 4 (≥ 80%).

unedited

2.3 Cell Culture and Transfection

HACAT cells were purchased from the National Infrastructure of Cell Line Resource (Shanghai, China) and cultured in DMEM medium containing 10% fetal bovine serum (FBS) (# KC001-01, KEL Biotechnology, USA) and 1% penicillin/streptomycin. SCC9 and SCC25 cells were obtained from Procell Life Science & Technology Co., Ltd. (Wuhan, China) and cultured in DMEM/F12 supplemented with 10% FBS, 1% penicillin/streptomycin, and 400 ng/mL hydrocortisone (complete growth medium provided by Procell). All cell lines were cultured at 37℃ in a humidified incubator containing 5% CO_2 and tested for mycoplasma contamination. Small-interfering RNA (siRNA) was transfected using Lipo3000 (Invitrogen, USA) at a concentration of 100 nM following the manufacturer's instructions, and cell function assays were performed 24 h after transfection. The sequences of the small interfering RNAs are listed in Table S1.

2.4 CCK-8 assays

HNSCC cells (2×10^3 cells/well) transfected with si-CXCL16 were cultured in 96-well plates and cell viability was detected at 0, 1, 2, 3, and 4 days. The cell counting kit-8 (CCK-8) (Vazyme Biotech Co., Ltd, Nanjing) consisted of 90 μL of culture medium and 10 μL of CCK-8 reagent. The mixture was kept at 37℃ with 5% CO_2 for 2 h, followed by incubation with a Synergy LX multi-mode reader (BioTek Instruments, USA) to measure the optical density (OD) at 450 nm.

In the GPX1 inhibitor assay, different groups of HNSCC cells (2×10^3 cells/well) transfected with si-CXCL16 were cultured in 96-well plates and treated with 2 μM ED-71 for 0, 24, 48, 72, and 96 h. Subsequent experiments were performed as previously described and the OD values were assayed.

2.5 Clone formation

Groups of si-CXCL16 cells (SCC9 and SCC25) were inoculated in 12-well plates at 2,000 cells/well and cultured at 37℃ for 1 week. The colony cells retained in the plates were fixed with 4% methanol for 20 min, then stained with 0.5% crystal violet, followed by the analysis of results.

In the GPX1 inhibitor assay, groups of si-CXCL16 cells (SCC9 and SCC25) were inoculated in 6-well plates at 5000/well, treated with 2 μM ED-71 and cultured for 1 week at 37°C, followed by the analysis of results.

2.6 Cell migration and invasion

Cell migration assays were performed using a modified Boyden chamber (Corning, 3422, USA). A total of 5×10^4 cells were suspended in 200 μL of serum-free DMEM/F12 and inoculated onto polycarbonate filters for migration assays, with each lower chamber filled with 600 μL of 10% FBS-DMEM/F12. For the invasion assay, matrix gel was diluted in serum-free DMEM/F12 at a ratio of 1:6, then the formulated matrix gel was wrapped around the upper chamber membrane and incubated at 37℃ for 3 hours. To assess the invasive ability of HNSCC, 1×10^5 cells in 200 μL of serum-free DMEM were placed into the upper chamber of wells coated with reconstituted matrix gel, while 600 μL of 10% FBS-DMEM/F12 was placed in the lower chamber. After 24 h of incubation, the cells that migrated or invaded the lower chamber were fixed with 1 mL 4% formaldehyde for 20 min and stained with 0.5% crystal violet for 30 min. Unmigrated cells in the upper chamber were removed and the chamber was washed with phosphate-buffered saline. Each well was randomly photographed using an EVOS M7000 Smart Imaging System (magnification, 20×; Thermo Fisher Scientific, USA) with at least three fields of view per well.

In the GPX1 inhibitor assay, groups of si-CXCL16 cells (SCC9 and SCC25) were inoculated in 6-well plates at 1.5×10^5 wells and cultured for 24 hours at an ED-71 concentration of 2 μM. Subsequently, inhibitor-pretreated cells were inoculated at 5×10^4 cells/well in the upper chamber, and 600 μL of 10% FBS-DMEM/F12 was placed in the lower chamber. The cells were incubated, followed by formaldehyde fixation, crystal violet staining, and were photographed.

unedited

2.7 Western blot

HNSCC cells from different groups were harvested using western blotting and IP lysis buffer (P0013, Beyotime Institute of Biotechnology, China) supplemented with protease and phosphatase inhibitors and lysed on ice for 10 min. Total protein concentration was determined using a bicinchoninic acid protein assay kit (Thermo Fisher Scientific, USA). The protein samples were separated using SDS-PAGE precast Tris-Gly gels (4-20%, 36270ES10, Yeasen Biotechnology, China) and transferred to PVDF membranes. The membranes were first incubated with 5% milk (Beijing Sola Biotechnology Co., Ltd.) for 1 h at room temperature, then overnight at 4°C with the following primary antibodies: anti-β-tublin (1:1000; AC030, ABclonal, China), anti-CXCL16 (1:1000; 60123-1-Ig, Proteintech, China), anti-N-cadherin (1:1000; 22018-1-AP, Proteintech, China), anti-E-cadherin (1:1000; 20874-1-AP, Proteintech, China), anti-NFE2L2 (1:1000; 80593-1-RR, Proteintech, China), anti-GPX1 (1:1000; A6-C0-B9-R, Huabio, China), and anti-GAPDH (1:1000; 60004-1-Ig, Proteintech, China). The membranes were washed three times and incubated with goat anti-rabbit IgG (1:3000; A0208, Beyotime, China) or anti-mouse IgG (1:3000; A0216, Beyotime, China) for 2 h at room temperature, then analyzed using an FDbioDura ECL kit (#FD8020, Fdbio Science, China) with a ChemiDoc-MP imager (Bio-Rad, USA).

2.8 Reverse transcription quantitative PCR (RT-qPCR)

Total cellular RNA was extracted using the TRIzol reagent and its concentration was measured using a NanoDrop spectrophotometer. The cDNA was obtained using the Evo M-MLV RT Premix for qPCR (AG11706, Accurate Biotechnology (Hunan) Co., Ltd., China) Reverse Transcription Kit, with the reverse transcription performed at 37℃ for 15 min and at 85℃ for 5 s. A qPCR assay was performed using a Premix Pro Taq HS qPCR Kit (ROX Plus) (AG11718, Accurate Biotechnology (Hunan) Co., Ltd., China) with reagents provided in

a protocol, yielding a total volume of 10 μL. The thermal cycling conditions were 95℃ for 1 min, followed by 40 cycles at 95℃ for 5 s and 60℃ for 30 s. Relative gene expression was determined by the $2^{-\Delta\Delta Ct}$ method using β-actin as an internal reference (Livak and Schmittgen, 2001) and the primers were listed in Table S2.

2.9 Measurement of intracellular ROS levels

Different groups of HNSCC cells (ED-71 final concentration of 10 μM, DMEM/F12 without FBS) were incubated with DCFH-DA (2,7-dichloro-hydroxyfluorescein diacetate) (# T15458, TargetMol, USA) for 30 min at 37℃ in a dark environment and subsequently washed twice with DMEM/F12 without FBS. Photographs were taken randomly in the dark with at least three fields of view per well using an EVOS M7000 Smart Imaging System (magnification: 20×; Thermo Fisher, USA).

2.10 Transcriptome gene analysis

SCC9 cells were cultured to achieve 70% confluency in 10 cm dishes and transfected with small interfering (si) RNA and lipo3000 (Invitrogen, USA) at a working concentration of 100 nM. Cells were collected after 48 h and analyzed using RNA-sequencing (Lianchuan Biotech Co., Ltd. Hangzhou, China).

2.11 ELISA

The concentration of CXCL16 in the culture medium of HACAT, SCC9 and SCC25 cells was analyzed using the Human CXCL16 ELISA Kit (MM-2133H1, Jiangsu Meimian Industrial Co., Ltd, China). All assays were performed according to the manufacturer's protocol.

2.12 Statistical analysis

Experimental data were presented as mean ± standard error (SEM). Overall survival (OS) was estimated using the Kaplan-Meier method. Differences between two groups were compared by the t-test. All experiments were performed with at least three replicates. Differences were considered significant when $P < 0.05$. Statistical analyses were performed using GraphPad Prism 8 statistical software (GraphPad Software, USA).

unedited

3 Results

3.1 Overexpressed CXCL16 in HNSCC tissues and cell lines

In order to investigate the role of CXCL16 in tumor development in patients with HNSCC, we analyzed the differences between HNSCC carcinoma and paracancer using the TCGA database. The database was classified into CXCL16 high-expression group (n=515) and low-expression group (n=44) according to the median level of CXCL16 in patients with HNSCC. The results revealed a significantly higher CXCL16 level in cancer tissues compared to adjacent normal tissues (Fig. 1a, $P < 0.01$). To assess the diagnostic significance of high CXCL16 expression in patients with HNSCC, we conducted a ROC curve analysis and found that CXCL16 could statistically differentiate HNSCC tissues from normal tissues, with an area under the curve (AUC) of 0.6015 (95% CI: 0.5094-0.6937; $P < 0.05$) (Fig. 1b). Subsequently, we evaluated the clinicopathological relationship between CXCL16 expression levels and HNSCC based on the primary tumor T-stage and the overall tumor stage. Each group was evaluated by a comparison between the two groups with the normal group. The findings demonstrated a positive correlation between high CXCL16 expression and advanced HNSCC tumor stage (Fig. 1c and 1d). The differential expression of CXCL16 did not significantly vary in terms of gender, distant metastasis, lymph node metastasis, and overall survival curves (Figs. S1a-1Sd). Next, we analyzed the relationship between the expression of CXCL16 and its clinical relevance in HNSCC tumors in the TCGA database, and found that high expression of CXCL16 in cancer tissues correlated with age and lymphovascular invasion (Table S3). To verify CXCL16 expression in tissue cancer versus paracancer in patients with HNSCC, we randomly selected a paracancer case from the cut margin tissue of a patient with a negative pathology report, as well as eleven pa-

tients with HNSCC, all of whom underwent immunohistochemical staining for CXCL16. We found that CXCL16 expression was significantly upregulated in patients with HNSCC compared to normal tissues (Fig. 1e). In addition, we assessed CXCL16 expression in normal epidermal HACAT cell lines and HNSCC cell lines through qPCR and western blotting, confirming its positive expression in cancer cells (Figs. 1f and 1g). We analyzed the release of soluble CXCL16 in HACAT, SCC9 and SCC25 cell lines by ELISA and revealed that the expression trend of the HNSCC cell lines was slightly higher than that of the normal epithelial HACAT cell line (Fig. S1e). In addition, the receptor CXCR6 for CXCL16 was found to be highly expressed in HNSCC cell lines and tumor patient tissues by qPCR and immunohistochemistry (Figs. S1f and S1g).

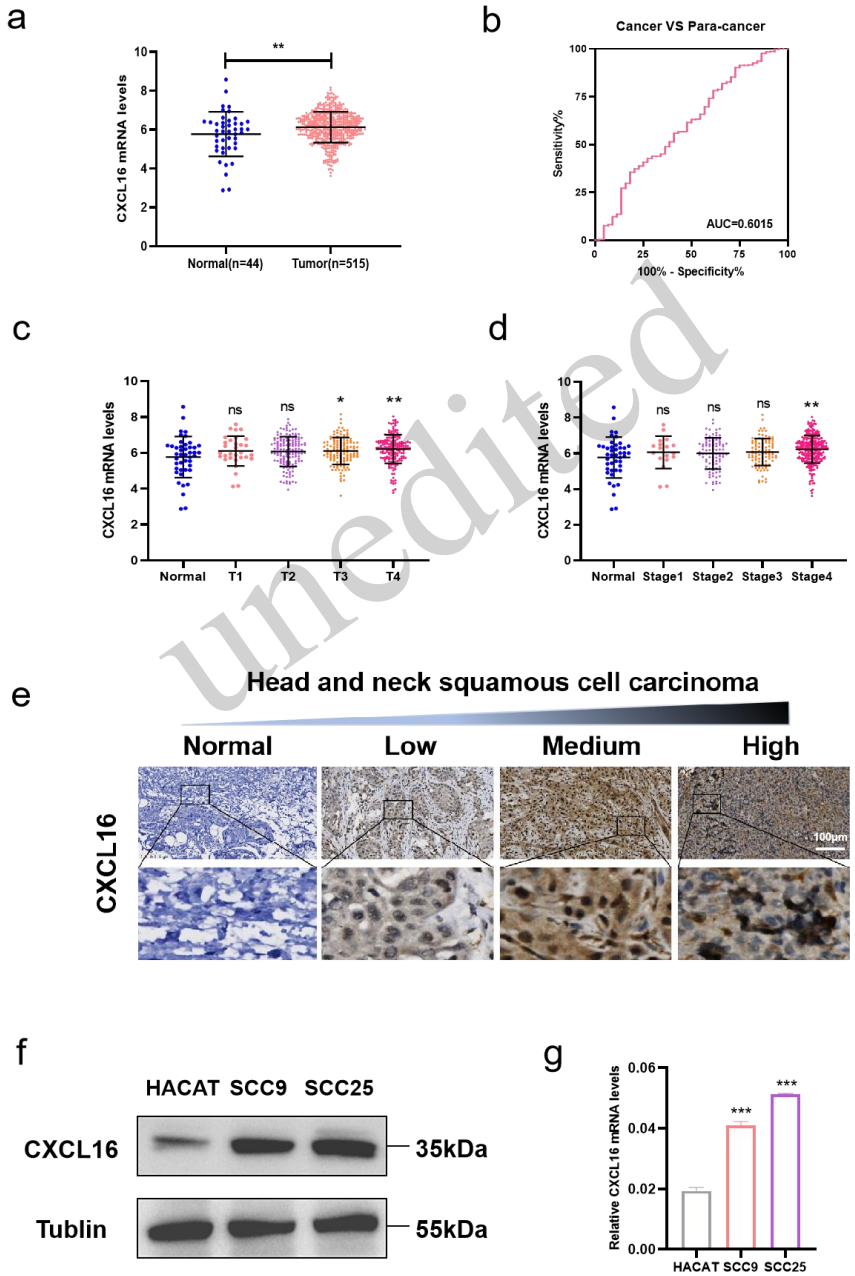

unedited

Fig. 1 CXCL16 is expressed at high levels in the tissues and cells of HNSCC patients. (a) Difference in mRNA expression levels of CXCL16 between tumor tissues and adjacent normal tissues from the TCGA database. (b) ROC curves showed that CXCL16 could effectively distinguish tumor tissue from adjacent normal tissue with an AUC of 0.6015. (c) Compar-

ison of the CXCL16 expression levels in the T staging of normal and tumor tissues from the TCGA database. (d) Comparison of CXCL16 expression levels in normal tissues with different stages of tumor tissues from the TCGA database. (e) Immunohistochemical results of CXCL16 in tumor tissues and adjacent normal tissues of patients with HNSCC from our central hospital (20×). Scale bar = 100 μm. (f) CXCL16 protein levels in normal epidermal cell lines (HACAT) and HNSCC cell lines (SCC9, SCC25). (g) Expression levels of CXCL16 mRNA in normal epidermal cell lines (HACAT) and HNSCC cell lines (SCC9, SCC25) (*n*=3). The data were expressed as mean±SEM, n=3. ns: no significance; $^{**}P < 0.01$; $^{*}P < 0.05$. CXCL16: CXC motif chemokine ligand 16; HNSCC: head and neck squamous carcinoma; mRNA: messenger RNA; TCGA: The Cancer Genome Atlas; ROC: receiver operating characteristic; AUC: area under curve; Tublin: β-Tubulin; SEM: standard error of mean.

3.2 Proliferation, migration, and invasion are inhibited in HNSCC cells by knockdown of CXCL16

In order to investigate the role of CXCL16 in HNSCC, we selected SCC9 and SCC25 cells with high CXCL16 expression as target cells and transfected them with si-CXCL16 to knock down the expression of CXCL16. The qPCR and western blotting results demonstrated that the knockdown efficiency of CXCL16 was as expected (Figs. 2a and 2b). Furthermore, we compared the si-CXCL16 group with the NC group and analyzed the difference. CXCL16 knockdown significantly affected the proliferation and clone formation of HNSCC cells (Figs. 2c and 2d). In addition, transwell experiments showed that migration and invasion were significantly inhibited in the CXCL16 knockdown group compared with the NC group (Figs. 2e and 2f). Next, we continued to explore the effect of CXCL16 on the EMT process in SCC9 and SCC25 cells by western blotting experiments, and found that the knockdown of CXCL16 inhibited EMT pathway transformation in SCC9 and SCC25 cell lines, the expression level of N-cadherin, a protein related to the EMT pathway, was reduced, while E-cadherin was elevated at the expression level (Fig. 2g).

unedited

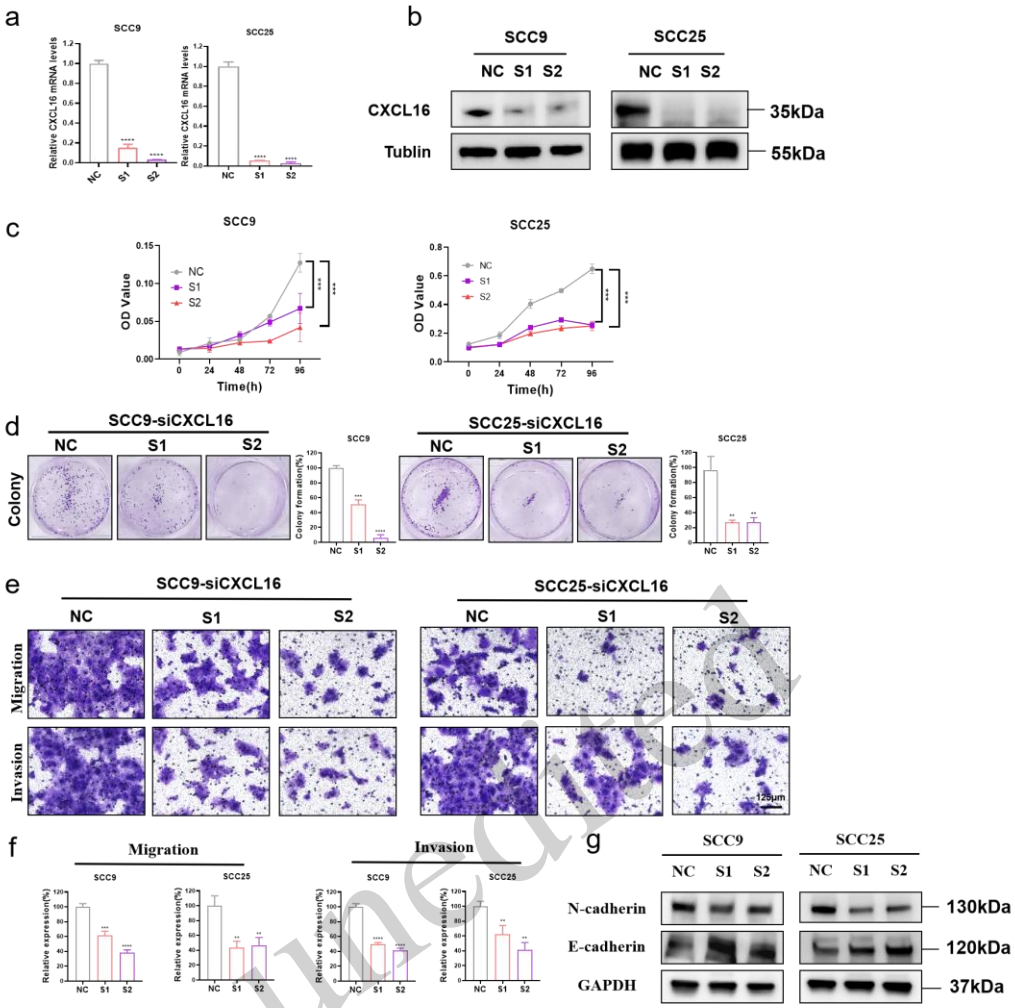

Fig. 2 CXCL16 promotes the proliferation, migration, and invasion of HNSCC cells. (a) mRNA level of CXCL16 after its knockdown in HNSCC cell lines (*n*=3). (b) Protein level expression of CXC16 after its knockdown in HNSCC cell lines. (c) Cell proliferation results (CCK8) of NC group compared to si-CXCL16 group (*n*=3). (d) Results of clone formation and the quantification of SCC9 and SCC25 cell line clone formation results and quantification plots (*n*=3). (e) SCC9 and SCC25 cell migration and invasion results. Scale bar = 125 μm. (f) Quantification graph of SCC9 and SCC25 cell migration and invasion (*n*=3). (g): Changes in EMT markers (E-cadherin, N-cadherin) in SCC9 and SCC25 cells after CXCL16 knockdown. The data were expressed as mean±SEM, n=3. ****P < 0.0001; ***P < 0.001; **P < 0.01. CXCL16: CXC motif chemokine ligand 16; HNSCC: head and neck squamous carcinoma; CCK8: cell counting kit-8; Tublin: β-Tubulin; si-CXCL16: small interfering CXCL16; NC: negative control; S1: si-CXCL16-1; S2: si-CXCL16-2; GAPDH: glyceraldehyde-3-phosphate dehydrogenase; EMT: epithelial-mesenchymal transition; SEM: standard error of mean.

unedited

3.3 HNSCC cells viability was promoted by CXCL16 through ROS action in the antioxidant pathway

In order to further explore the potential molecular mechanisms of CXCL16, we conducted RNA transcriptomic analysis of CXCL16 in HNSCC cells (Fig. 3a). The Gene Ontology (GO) pathway enrichment results showed a significant difference in antioxidant activity between the si-CXCL16 and NC group (Fig. 3b). The analysis of differentially expressed genes revealed that PLAU, AXL, CXCL16, POP7, ICAM1, GPX1, EPHA2, GAS6, ITGB4, and BSG, associated with migratory invasion outcomes, were significantly downregulated in the si-CXCL16 group (Figs. 3c-3e). According to the results for Protein-Protein Interaction Networks (PPI), GPX1 acts as a downstream hub gene of CXCL16 in regulating the migration and invasion of HNSCC cells (Fig. 3f).

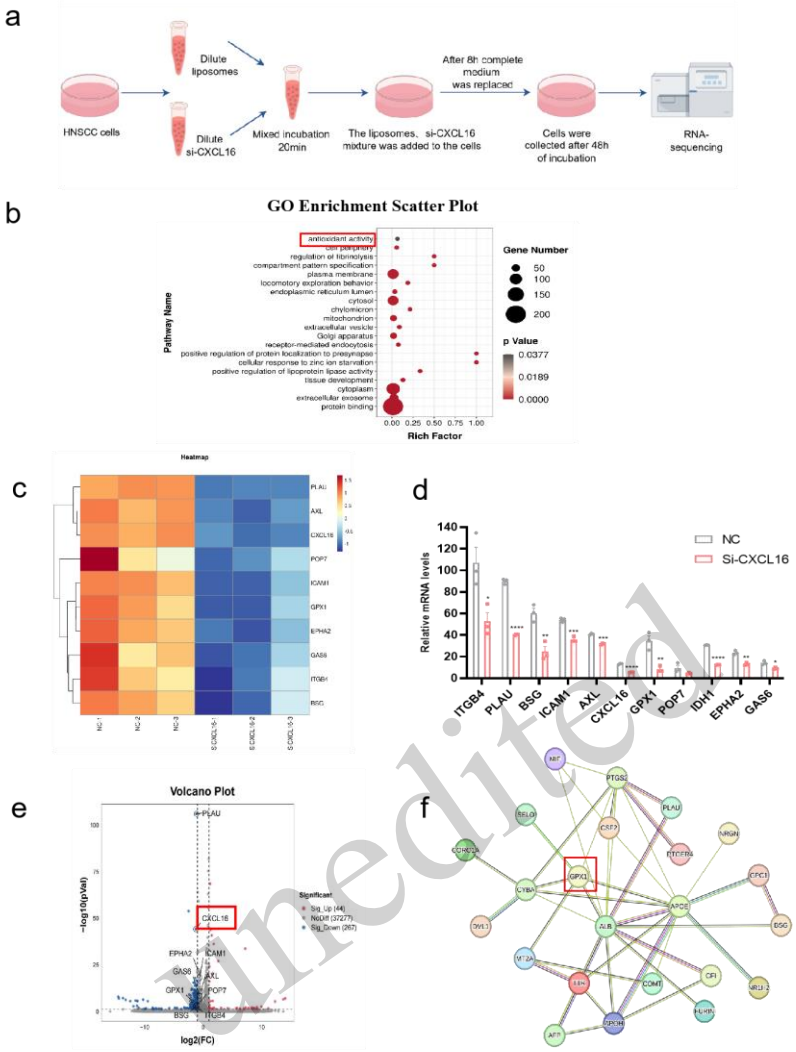

Unedited

Fig. 3 Transcriptome sequencing analysis after knockdown of CXCL16. (a) Schematic diagram of the RNA-sequencing steps (By Figdraw). (b) GO pathway enrichment analysis showed that the antioxidant pathway was enriched. (c) Differential gene expression heatmap (PLAU, AXL, CXCL16, POP7, ICAM1, GPX1, EPHA2, GAS6, ITGB4, BSG). (d) Quantitative graph of differential gene expression (*n*=3). (e) Volcano plot showing differentially expressed genes of si-CXCL16 and NC. Upregulated genes and downregulated genes are marked in red and blue, respectively. (f): PPI protein interaction map analysis showing the enrichment of antioxidant gene GPX1. The data were expressed as mean±SEM, n=3. ****P < 0.0001; ***P < 0.001; **P < 0.01; *P < 0.05. CXCL16: CXC motif chemokine ligand 16; HNSCC: head and neck squamous carcinoma; GO: Gene Ontology; si-CXCL16: small interfering CXCL16; NC: negative control; PPI: protein protein interaction network; ITGB4: Integrin β4; PLAU: The urokinase-type plasminogen activator; BSG: borosilicate glass; ICAM1: intercellular adhesion molecule-1; AXL: AXL receptor tyrosine kinase Gene; GPX1: glutathione peroxidase 1; POP7: processing of precursor 7; IDH1: isocitrate dehydrogenase1; EPHA2: ephrin receptor A2; GAS6: growth arrest-specific 6; SEM: standard error of mean.

To validate the results of transcriptome analysis, we compared the RNA levels of the si-CXCL16 group with the NC group. The results showed a significant downregulation of PLAU, AXL, CXCL16, POP7, ICAM1, GPX1, EPHA2, GAS6, ITGB4, and BSG in the si-CXCL16 group, consistent with the transcriptome results (Fig. 4a). In addition, we randomly selected four unregulated genes from the transcriptome results and they were

as expected based on qPCR (Fig. S2). Certain studies have confirmed that the antioxidant-related genes Nfe2l2, SOD1, SOD2, GSR, NQO1, GSS, and GCLM play key roles in inflammatory responses and cancer development (Becker and Juvik, 2016; Mei et al., 2020; Tsai et al., 2021; Wu et al., 2021; Kassab et al., 2023). Our study also revealed that the mRNA levels of Nfe2l2, SOD1, SOD2, GSR, NQO1, GSS, and GCLM were significantly downregulated in the si-CXCL16 group compared to the NC group (Figs. 4b and 4c). Furthermore, the trend of ROS upregulation was similar in SCC9 and SCC25 cell lines after CXCL16 knockdown (Figs. 4d and 4e).

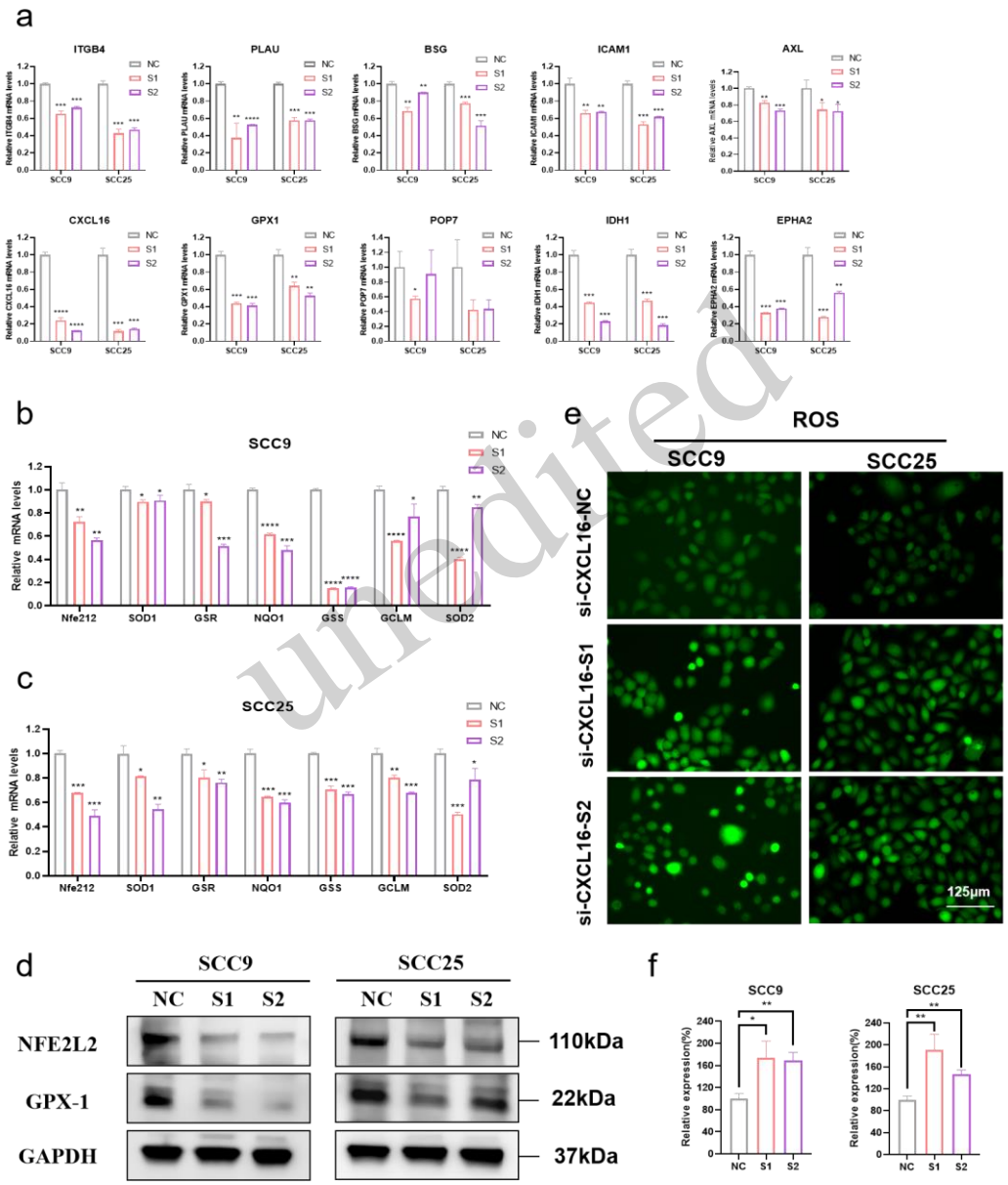

unedited

Fig. 4 CXCL16 promotes HNSCC development via an antioxidant pathway. (a) The si-CXCL16 group vs. the NC group were evaluated in a two-group comparison to validate the mRNA expression levels of differential genes associated with migration, invasion and antioxidation (*n*=3). (b) The si-CXCL16 group was compared with the NC group in the mRNA expression levels of antioxidant-related genes in SCC9 (*n*=3). (c) The si-CXCL16 group was compared with the NC group for the mRNA expression levels of antioxidant-related genes in SCC25 cells (*n*=3). (d) ROS levels were significantly increased after the knockdown of CXCL16 in SCC9 and SCC25 cell lines. Scale bar = 125 μm. (e) Quantitative graph of

ROS levels in SCC9 and SCC25 after the knockdown of CXCL16 (*n*=3). The data were expressed as mean±SEM, n=3. *******P* < 0.0001; ******P* < 0.001; *****P* < 0.01; ****P* < 0.05. CXCL16: CXC motif chemokine ligand 16; si-CXCL16: small interfering CXCL16; mRNA: messenger RNA; NC: negative control; S1: si-CXCL16-1; S2: si-CXCL16-2; ROS: reactive oxygen species; ITGB4: Integrin β4; PLAU: The urokinase-type plasminogen activator; BSG: borosilicate glass; ICAM1: intercellular adhesion molecule-1; AXL: AXL receptor tyrosine kinase Gene; GPX1: glutathione peroxidase 1; POP7: processing of precursor 7; IDH1: isocitrate dehydrogenase1; EPHA2: ephrin receptor A2; Nfe2l2: nuclear factor, erythroid 2-like 2; SOD1: superoxide dismutase 1; SOD2: superoxide dismutase 2; GSR: glutathione reductase; GSS: glutathione synthetase; NQO1: NADPH quinone oxidoreductase 1; GCLM: glutamate-cysteine ligase modifier subunit; SEM: standard error of mean.

3.4 HNSCC cells growth was promoted by CXCL16-GPX1 signaling way

In order to further verify that CXCL16 regulates HNSCC cell viability through GPX1, we used ED-71, a GPX1 inhibitor, combined with si-CXCL16 treated HNSCC cells. We compared the ED-71 and si-CXCL16 combined group with the si-CXCL16 alone group, and found that the combination of ED-71 and si-CXCL16 significantly inhibited the proliferation of SCC9 and SCC25 cells (Fig. 5a). In cell migration assays, it was also indicated that ED-71 combined with si-CXCL16 inhibited the migratory ability of HNSCC cell lines relative to the si-CXCL16 alone group (Figs. 5b and 5c). The clone formation results showed that the inhibition of GPX1 significantly suppressed cell clone formation (Figs. 5d, S3a and S3b). We next verified the changes in antioxidant gene mRNA levels in the ED-71 and si-CXCL16 combined group versus the si-CXCL16 alone group. Nfe2l2, GSR, NQO1, and GSS levels were more significantly downregulated in the ED-71 combined with the si-CXCL16 group (Fig. 5e). Western blotting experiments unveiled that the expression levels of GPX1 and NFE2L2 proteins were also downregulated in SCC9 and SCC25 cells (Fig. 5f). In addition, the ED-71 combined with si-CXCL16 group showed a similar trend toward the upregulation of ROS levels, indicating that knockdown of the expression of CXCL16 inhibited the growth of HNSCC cells through the GPX1 signaling axis (Figs. 5g and 5h).

unedited

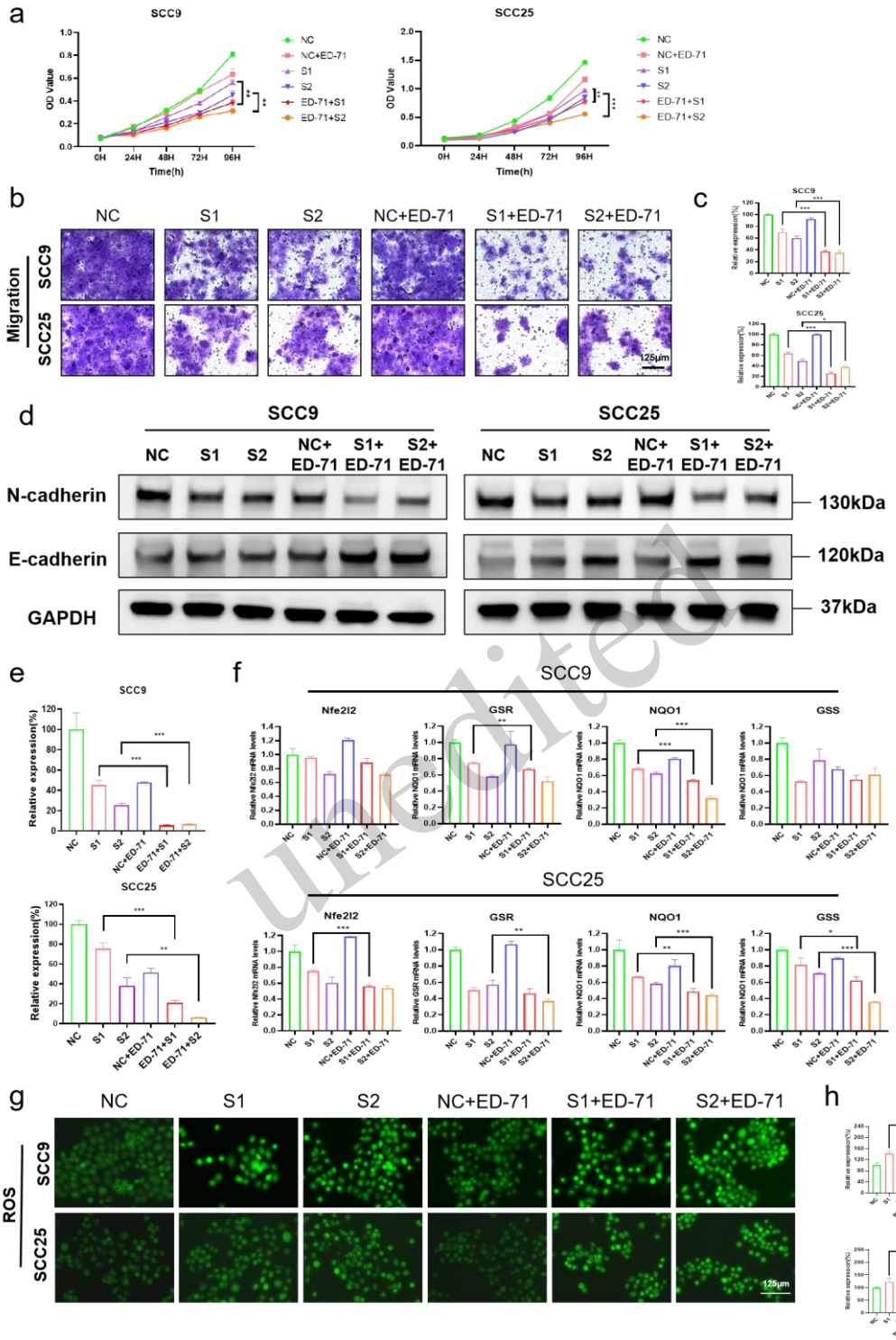

unedited

Fig. 5 CXCL16 promotes the development of HNSCC cells through GPX1. (a) The ED-71 and si-CXCL16 combination group was compared with the si-CXCL16 alone group. The combination of ED-71 and si-CXCL16 inhibited the proliferation of HNSCC cells (*n*=3). (b) Migration results of the inhibition of SCC9 and SCC25 cell lines after 48 hours of cell incubation by ED-71 and si-CXCL16. Scale bar = 125 μm. (c) Quantification graph of ED-71 and si-CXCL16 co-action migration (*n*=3). (d) Quantification graph of clone formation in SCC9 and SCC25 cells after ED-71 and si-CXCL16 co-action (*n*=3). (e) The combination group of ED-71 and si-CXCL16 was compared with the si-CXCL16 alone group and the mRNA expression levels of antioxidant-related genes (Nfe2l2, GSR, NQO1, GSS) were suppressed in HNSCC cells

(*n*=3). (f) Changes in the protein levels of antioxidant-related genes GPX1, NFE2L2 in SCC9 and SCC25 cell lines after the co-action of ED-71 and si-CXCL16. (g) Increased ROS levels in SCC9 and SCC25 cell lines after the co-action of ED-71 and si-CXCL16. Scale bar = 125 μm. (h) Quantitative graphs of ROS levels in SCC9 and SCC25 cell lines after the co-action of ED-71 and si-CXCL16 (*n*=3). The data were expressed as mean±SEM, n=3. ns: no significance; ****P* < 0.001; ***P* < 0.01; **P* < 0.05. CXCL16: CXC motif chemokine ligand 16; HNSCC: head and neck squamous carcinoma; ED-71: eldecalcitol; si-CXCL16: small interfering CXCL16; NC: negative control; S1: si-CXCL16-1; S2: si-CXCL16-2; ROS: reactive oxygen species; NFE2L2: nuclear factor, erythroid 2-like 2; GSR: glutathione reductase; NQO1: NADPH quinone oxidoreductase 1; GSS: glutathione synthetase; GPX1: glutathione peroxidase 1; GAPDH: glyceraldehyde-3-phosphate dehydrogenase; SEM: standard error of mean.

4 Discussion

HNSCC is a major malignant tumor, characterized by high recurrence and metastasis rates. Therefore, identifying effective prognostic biomarkers and therapeutic targets for patients with HNSCC is of high urgency. Many clinical predictors of HNSCC are slowly coming into public view. In addition to immune checkpoint inhibitor treatments, other novel biomarker molecules have also been reported to be potential therapeutic targets, such as NRF2 and PYGL, which are related to cellular metabolism (Tang et al., 2021; Guan et al., 2023). Although recent studies have shown significant progress in the genomic and immunotherapeutic aspects of HNSCC, few molecules can be applied in clinical practice (Ruffin et al., 2023), leaving surgery and radiotherapy the main treatment options for HNSCC at present. The treatment of advanced HNSCC in the course of clinical treatment has been associated with a very high rate of resistance, the frequent recurrence of which has led to poor therapeutic effects in HNSCC (Jiang et al., 2022). Chemokines play an important role as mediators of intercellular communication, as they can recruit immune cells to generate an immune response, regulate tumor cells' migration and invasion, and influence tumor development (Liu et al., 2020; Khan et al., 2022). CXCL16 plays a vital role in angiogenesis, the tumor immune microenvironment, and promoting tumor cells' proliferation, migration, invasion, metastasis and EMT transformations (Korbecki et al., 2021). CXCL16 was found to cause kidney damage and cardiovascular disease; elevated CXCL16 levels promoted the development of prostate cancers (Izquierdo et al., 2014; Richardsen et al., 2015). It has been found that the CXCL16-CXCR6 signaling axis induces the migration and invasive ability of colorectal cancer and osteosarcoma cells and promotes the transformation of the EMT pathway, and that osteosarcoma results primarily from activation of CXCR6 via the AKT pathway (Matsushita et al., 2012; Ma et al., 2017). However, the biological function and molecular mechanism of CXCL16 in head and neck squamous carcinoma are still unclear.

Our study established that the expression of CXCL16 was upregulated in HNSCC patients through TCGA database analysis (Fig. 1a). We also observed that high expression of CXCL16 was positively correlated with tumor T3 and T4 stages (Fig. 1c). ROC curve analysis revealed that high CXCL16 expression effectively distinguished HNSCC from individuals without malignancy (Fig. 1b). To confirm the accuracy of the cancer database, we examined CXCL16 expression in patient tissues and HNSCC cell lines, and the results were consistent with the database predictions (Figs. 1e-1g). Subsequently, we investigated the role of CXCL16 in HNSCC cells and utilized small interfering RNS to knock down CXCL16 expression in these cells. The knockdown of CXCL16 inhibited the migration and invasive abilities of HNSCC cells (Fig. 2), indicating that CXCL16 may be a promising candidate target molecule in HNSCC patients.

Subsequently, the transcriptome analysis indicated that the cellular antioxidant pathway was altered and the antioxidant-related gene GPX1 was downregulated (Fig. 3d). According to previous reports, GPX1 interacts with superoxide dismutase and catalase to form an enzymatic antioxidant system that reduces ROS and limit their toxicity. It can be involved in tumor biology through various pathways, such as cell proliferation, apoptosis, invasion, and immune response (Zhao et al., 2022; Pei et al., 2023). Upregulation of GPX1 expression correlates with poor prognosis in glioblastoma, and cellular and exosomal GPX1 are critical for controlling hydrogen peroxide homeostasis and attenuating oxidative stress in hypoxic glioblastoma (Lei et al., 2023). In hepatocellular carcinoma, reduced selenium-binding protein 1 promotes hepatocellular carcinoma invasion by en-

Unedited

hancing GPX1 activity and decreasing HIF-1α expression (Huang et al., 2012). Herein, we used ED-71 (GPX1 inhibitor) combined with si-CXCL16 treated with HNSCC cells to verify the effect of CXCL16 on the viability of HNSCC cells via GPX1 (Fig. 5). ROS accumulation causes DNA damage, genetic instability, metabolic adaptation, drug resistance, and cell death (Moloney and Cotter, 2018). According to our experimental results, knockdown of the expression of CXCL16 affected the increase in ROS levels in HNSCC cells by regulating the level of GPX1, resulting in a diminished ability of cells to undergo value addition, migration and invasion.

5 Conclusions

In summary, our results indicate that CXCL16 is highly expressed in the HNSCC tissues and is associated with poor prognosis. In terms of the underlying mechanism, high expression of CXCL16 promotes migration and invasion ability of HNSCC cells by regulating the level of antioxidant gene GPX1 (Fig. 6). Our study provides a new direction for treating HNSCC and highlights the potential value of CXCL16 as a new diagnostic target for HNSCC.

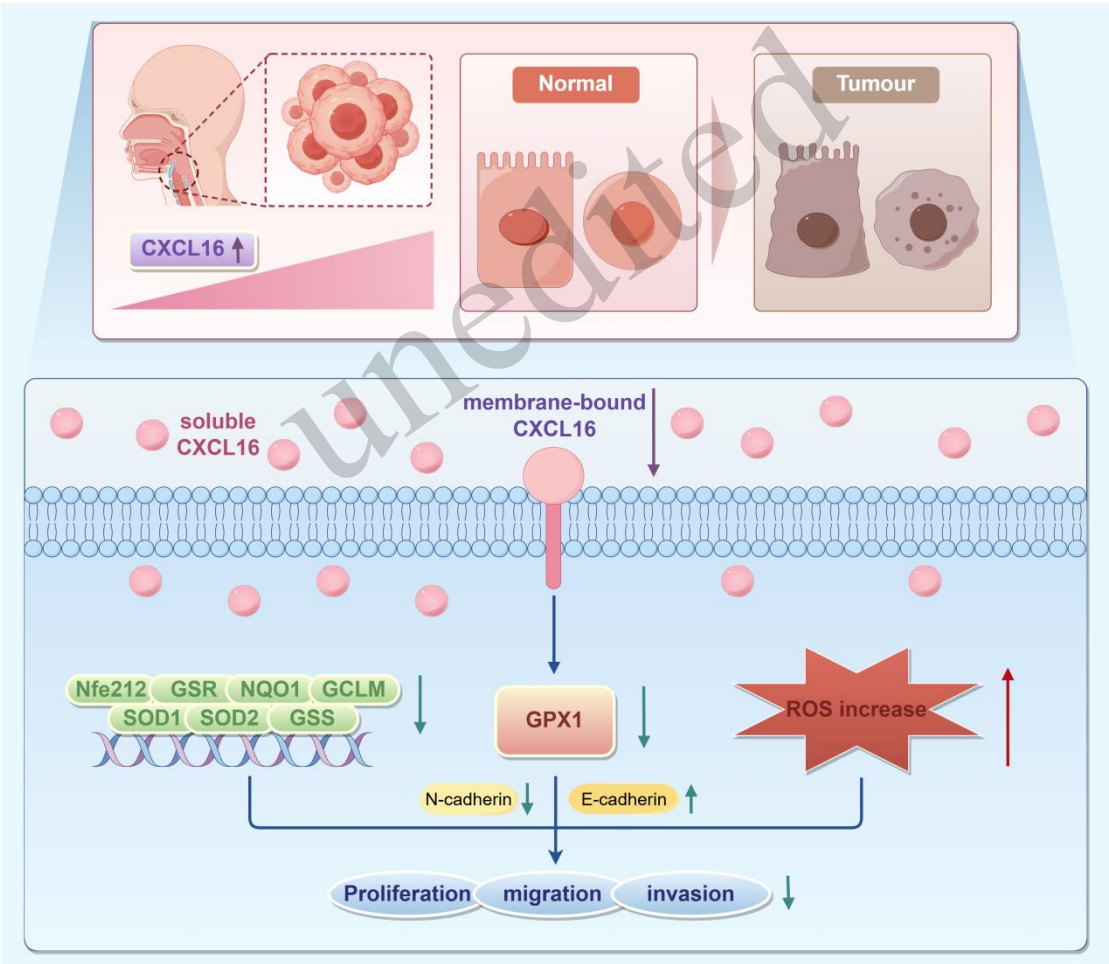

unedited

Fig. 6 Schematic representation of CXCL16 promoting HNSCC development through GPX1 (By Figdraw). CXCL16 promotes HNSCC tumor development by regulating GPX1-mediated antioxidant levels. Nfe2l2: nuclear factor, erythroid 2-like 2; SOD1: superoxide dismutase 1; SOD2: superoxide dismutase 2; GSR: glutathione reductase; GSS: glutathione synthetase; NQO1: GCLM: glutamate-cysteine ligase modifier subunit; GPX1: glutathione peroxidase 1; ROS: reactive oxygen species.

Data availability statement

All datasets analyzed in this study are available from the corresponding author upon request.

Acknowledgments

This work was supported by the Scientific Research Fund of the National Health Commission -- Zhejiang Provincial Health Major science and technology Plan project (WKJ-ZJ-2415), the Key Research and Development Program of Zhejiang Province (2024C03166), the Traditional Chinese Medicine Science and Technology Project of Zhejiang Province (grant number 2022ZB020), and the Zhejiang Provincial Natural Science Foundation (grant number LY21H160049). We also thank Figdraw (www.figdraw.com) for the assistance in creating Scheme.

Author contributions

All authors contributed to the study's conception and design. Ru He and Hongyi Jiang designed the experiment and drafted the manuscript. Chengchi Zhang, Yuan Chen, Wenshun Liu, Yunye Liu, Yining Zhang, and Chengying Shao performed the study. Xinyue Deng, Xiaozheng Zhu, and Chuanming Zheng analyzed data. Yanting Duan and Jiajie Xu designed the experiment, revised the manuscript, and monitored the project progression. All authors have read and approved the final manuscript, and therefore, have full access to all the data in the study and took responsibility for the integrity and security of the data.

Compliance with ethics guidelines

Ru He, Hongyi Jiang, Chengchi Zhang, Yuan Chen, Wenshun Liu, Xinyue Deng, Xiaozheng Zhu, Yunye Liu, Chuanming Zheng, Yining Zhang, Chengying Shao, Yanting Duan, Jiajie Xu declare that they have no conflicts of interest.

All patients were informed of sample collection and use. Tissue samples were collected and used according to the protocols approved by the Human Research Ethics Committee of Zhejiang Provincial People's Hospital. This study was conducted in accordance with the Declaration of Helsinki and national and international guidelines (Acceptance Number: QT2024066).

unedited

References

Abel S, Hundhausen C, Mentlein R, et al., 2004. The transmembrane CXC-chemokine ligand 16 is induced by IFN-gamma and TNF-alpha and shed by the activity of the disintegrin-like metalloproteinase ADAM10. *J Immunol*, 172(10):6362-6372. https://doi.org/10.4049/jimmunol.172.10.6362

Becker TM, Juvik JA, 2016. The role of glucosinolate hydrolysis products from brassica vegetable consumption in inducing antioxidant activity and reducing cancer incidence. *Diseases*, 4(2):22. https://doi.org/10.3390/diseases4020022

Bray F, Ferlay J, Soerjomataram I, et al., 2018. Global cancer statistics 2018: GLOBOCAN estimates of incidence and mortality worldwide for 36 cancers in 185 countries. *Ca Cancer J Clin*, 68(6):394-424. https://doi.org/10.3322/caac.21492

Brockstein B, Haraf DJ, Rademaker AW, et al., 2004. Patterns of failure, prognostic factors and survival in locoregionally advanced head and neck cancer treated with concomitant chemoradiotherapy: a 9-year, 337-patient, multi-institutional experience. *Ann Oncol*, 15(8):1179-1186. https://doi.org/10.1093/annonc/mdh308

Chalabi-Dchar M, Cassant-Sourdy S, Duluc C, et al., 2015. Loss of somatostatin receptor subtype 2 promotes growth of KRAS-induced pancreatic tumors in mice by activating PI3K signaling and overexpression of CXCL16. *Gastroenterology*, 148(7):1452-1465. https://doi.org/10.1053/j.gastro.2015.02.009

Cho SW, Kim YA, Sun HJ, et al., 2016. CXCL16 signaling mediated macrophage effects on tumor invasion of papillary thyroid carcinoma. *Endocr Relat Cancer*, 23(2):113-124. https://doi.org/10.1530/ERC-15-0196

Collado A, Marques P, Escudero P, et al., 2018. Functional role of endothelial CXCL16/CXCR6-platelet-leucocyte axis in angiotensin II-associated metabolic disorders. *Cardiovasc Res*, 114(13):1764-1775. https://doi.org/10.1093/cvr/cvy135

Dequanter D, Dok R, Koolen L, et al., 2017. Prognostic significance of glutathione peroxidase levels (GPx1) in head and neck cancers. *Front Oncol*, 7:84. https://doi.org/10.3389/fonc.2017.00084

Fan S, Tang QL, Lin YJ, et al., 2011. A review of clinical and histological parameters associated with contralateral neck metastases in oral squamous cell carcinoma. *Int J Oral Sci*, 3(4):180-191. https://doi.org/10.4248/IJOS11068

Griffith JW, Sokol CL, Luster AD, 2014. Chemokines and chemokine receptors: positioning cells for host defense and immunity. *Annu Rev Immunol*, 32:659-702.

https://doi.org/10.1146/annurev-immunol-032713-120145
Guan J, Xu X, Qiu G, et al., 2023. Cellular hierarchy framework based on single-cell/multi-patient sample sequencing reveals metabolic biomarker PYGL as a therapeutic target for HNSCC. *J Exp Clin Cancer Res*, 42(1):162. https://doi.org/10.1186/s13046-023-02734-w
Han J, Fu R, Chen C, et al., 2021. CXCL16 promotes gastric cancer tumorigenesis via ADAM10-dependent CXCL16/CXCR6 axis and activates Akt and MAPK signaling pathways. *Int J Biol Sci*, 17(11):2841-2852. https://doi.org/10.7150/ijbs.57826
Hattermann K, Gebhardt H, Krossa S, et al., 2016. Transmembrane chemokines act as receptors in a novel mechanism termed inverse signaling. *Elife*, 5:e10820. https://doi.org/10.7554/eLife.10820
Hsieh CY, Lin CC, Huang YW, et al., 2022. Macrophage secretory IL-1beta promotes docetaxel resistance in head and neck squamous carcinoma via SOD2/CAT-ICAM1 signaling. *Jci Insight*, 7(23):e157285. https://doi.org/10.1172/jci.insight.157285
Hu W, Liu Y, Zhou W, et al., 2014. CXCL16 and CXCR6 are coexpressed in human lung cancer in vivo and mediate the invasion of lung cancer cell lines in vitro. *Plos One*, 9(6):e99056. https://doi.org/10.1371/journal.pone.0099056
Huang C, Ding G, Gu C, et al., 2012. Decreased selenium-binding protein 1 enhances glutathione peroxidase 1 activity and downregulates HIF-1α to promote hepatocellular carcinoma invasiveness. *Clin Cancer Res*, 18(11):3042-3053. https://doi.org/10.1158/1078-0432.CCR-12-0183
Izquierdo MC, Martin-Cleary C, Fernandez-Fernandez B, et al., 2014. CXCL16 in kidney and cardiovascular injury. *Cytokine Growth Factor Rev*, 25(3):317-325. https://doi.org/10.1016/j.cytogfr.2014.04.002
Jiang Y, Guo H, Tong T, et al., 2022. lncRNA lnc-POP1-1 upregulated by VN1R5 promotes cisplatin resistance in head and neck squamous cell carcinoma through interaction with MCM5. *Mol Ther*, 30(1):448-467. https://doi.org/10.1016/j.ymthe.2021.06.006
Karaki S, Blanc C, Tran T, et al., 2021. CXCR6 deficiency impairs cancer vaccine efficacy and CD8+ resident memory T-cell recruitment in head and neck and lung tumors. *J Immunother Cancer*, 9(3):e1948. https://doi.org/10.1136/jitc-2020-001948
Kassab RB, Elhenawy AA, Abdulrahmantheyab, et al., 2023. Modulation of inflammatory, oxidative, and apoptotic stresses mediates the renoprotective effect of daidzein against glycerol-induced acute kidney injury in rats. *Environ Sci Pollut Res Int*, 30(56):119016-119033. https://doi.org/10.1007/s11356-023-30461-4
Khan P, Fatima M, Khan MA, et al., 2022. Emerging role of chemokines in small cell lung cancer: road signs for metastasis, heterogeneity, and immune response. *Semin Cancer Biol*, 87:117-126. https://doi.org/10.1016/j.semcancer.2022.11.005
Kim MJ, Sun HJ, Song YS, et al., 2019. CXCL16 positively correlated with M2-macrophage infiltration, enhanced angiogenesis, and poor prognosis in thyroid cancer. *Sci Rep*, 9(1):13288. https://doi.org/10.1038/s41598-019-49613-z
Korbecki J, Bajdak-Rusinek K, Kupnicka P, et al., 2021. The role of CXCL16 in the pathogenesis of cancer and other diseases. *Int J Mol Sci*, 22(7):3490. https://doi.org/10.3390/ijms22073490
Lei FJ, Chiang JY, Chang HJ, et al., 2023. Cellular and exosomal GPx1 are essential for controlling hydrogen peroxide balance and alleviating oxidative stress in hypoxic glioblastoma. *Redox Biol*, 65:102831. https://doi.org/10.1016/j.redox.2023.102831
Lepore F, D'Alessandro G, Antonangeli F, et al., 2018. CXCL16/CXCR6 axis drives microglia/macrophages phenotype in physiological conditions and plays a crucial role in glioma. *Front Immunol*, 9:2750. https://doi.org/10.3389/fimmu.2018.02750
Liu H, Wang G, Wu T, et al., 2022. Efficacy and Safety of Eldecalcitol for Osteoporosis: A Meta-Analysis of Randomized Controlled Trials. *Front Endocrinol (Lausanne)*, 13:854439. https://doi.org/10.3389/fendo.2022.854439
Liu H, Yang Z, Lu W, et al., 2020. Chemokines and chemokine receptors: A new strategy for breast cancer therapy. *Cancer Med*, 9(11):3786-3799. https://doi.org/10.1002/cam4.3014
Livak KJ, Schmittgen TD, 2001. Analysis of relative gene expression data using real-time quantitative PCR and the 2(-Delta Delta C(T)) method. *Methods*, 25(4):402-408. https://doi.org/10.1006/meth.2001.1262
Lu Y, Kou Y, Gao Y, et al., 2023. Eldecalcitol inhibits the progression of oral cancer by suppressing the expression of GPX-1. *Oral*

unedited

Dis, 29(2):615-627.
https://doi.org/10.1111/odi.14010

Ma Y, Xu X, Luo M, 2017. CXCR6 promotes tumor cell proliferation and metastasis in osteosarcoma through the Akt pathway. *Cell Immunol*, 311:80-85.
https://doi.org/10.1016/j.cellimm.2016.11.001

Matloubian M, David A, Engel S, et al., 2000. A transmembrane CXC chemokine is a ligand for HIV-coreceptor Bonzo. *Nat Immunol*, 1(4):298-304.
https://doi.org/10.1038/79738

Matsushita K, Toiyama Y, Tanaka K, et al., 2012. Soluble CXCL16 in preoperative serum is a novel prognostic marker and predicts recurrence of liver metastases in colorectal cancer patients. *Ann Surg Oncol*, 19 Suppl 3:S518-S527.
https://doi.org/10.1245/s10434-011-1993-8

Mei X, Qi D, Zhang T, et al., 2020. Inhibiting MARSs reduces hyperhomocysteinemia-associated neural tube and congenital heart defects. *Embo Mol Med*, 12(3):e9469.
https://doi.org/10.15252/emmm.201809469

Mei Z, Huang J, Qiao B, et al., 2020. Immune checkpoint pathways in immunotherapy for head and neck squamous cell carcinoma. *Int J Oral Sci*, 12(1):16.
https://doi.org/10.1038/s41368-020-0084-8

Moloney JN, Cotter TG, 2018. ROS signalling in the biology of cancer. *Semin Cell Dev Biol*, 80:50-64.
https://doi.org/10.1016/j.semcdb.2017.05.023

Moreira D, Sampath S, Won H, et al., 2021. Myeloid cell – targeted STAT3 inhibition sensitizes head and neck cancers to radiotherapy and T cell – mediated immunity. *J Clin Invest*, 131(2):e137001.
https://doi.org/10.1172/JCI137001

Pei J, Pan X, Wei G, et al., 2023. Research progress of glutathione peroxidase family (GPX) in redoxidation. *Front Pharmacol*, 14:1147414.
https://doi.org/10.3389/fphar.2023.1147414

Richardsen E, Ness N, Melbø-Jørgensen C, et al., 2015. The prognostic significance of CXCL16 and its receptor C-X-C chemokine receptor 6 in prostate cancer. *Am J Pathol*, 185(10):2722-2730.
https://doi.org/10.1016/j.ajpath.2015.06.013

Ruffin AT, Li H, Vujanovic L, et al., 2023. Improving head and neck cancer therapies by immunomodulation of the tumour microenvironment. *Nat Rev Cancer*, 23(3):173-188.
https://doi.org/10.1038/s41568-022-00531-9

Saddawi-Konefka R, O Farrell A, Faraji F, et al., 2022. Lymphatic-preserving treatment sequencing with immune checkpoint inhibition unleashes cDC1-dependent antitumor immunity in HNSCC. *Nat Commun*, 13(1):4289.
https://doi.org/10.1038/s41467-022-31941-w

Siegel RL, Miller KD, Jemal A, 2020. Cancer statistics, 2020. *Ca Cancer J Clin*, 70(1):7-30.
https://doi.org/10.3322/caac.21590

Siu LL, Even C, Mesia R, et al., 2019. Safety and efficacy of durvalumab with or without tremelimumab in patients with PD-L1-low/negative recurrent or metastatic HNSCC: the phase 2 CONDOR randomized clinical trial. *Jama Oncol*, 5(2):195-203.
https://doi.org/10.1001/jamaoncol.2018.4628

Tang YC, Hsiao JR, Jiang SS, et al., 2021. c-MYC-directed NRF2 drives malignant progression of head and neck cancer via glucose-6-phosphate dehydrogenase and transketolase activation. *Theranostics*, 11(11):5232-5247.
https://doi.org/10.7150/thno.53417

Tsai CF, Chen GW, Chen YC, et al., 2021. Regulatory effects of quercetin on M1/M2 macrophage polarization and oxidative/antioxidative balance. *Nutrients*, 14(1):67.
https://doi.org/10.3390/nu14010067

Wu W, Geng Z, Bai H, et al., 2021. Ammonium ferric citrate induced ferroptosis in non-small-cell lung carcinoma through the inhibition of GPX4-GSS/GSR-GGT axis activity. *Int J Med Sci*, 18(8):1899-1909.
https://doi.org/10.7150/ijms.54860

Zhao Y, Wang H, Zhou J, et al., 2022. Glutathione Peroxidase GPX1 and Its Dichotomous Roles in Cancer. *Cancers (Basel)*, 14(10):2560.
https://doi.org/10.3390/cancers14102560

Supplementary information

Table S1 si-CXCL16 sequences.

unedited

Table S2 Primer sequence.

Table S3 Analysis of clinical correlation between the expression of tumor CXCL16 and disease in patients with head and neck squamous carcinoma from the TCGA database.

Fig. S1 Differential expression of CXCL16 in clinical features and expression levels of CXCR6 between HNSCC cell lines and cancer tissues. (a): Relationship between CXCL16 expression level and gender difference from the TCGA database. (b): Relationship between CXCL16 expression level and M staging from the TCGA database. (c): Relationship between CXCL16 expression level and N staging from the TCGA database. (d): Association between CXCL16 expression and overall survival in HNSCC patients. (e): The expression level of soluble CXCL16 was detected by taking supernatants from HACAT, SCC9 and SCC25 cells after 24 hours of culture (n=3). (f): Expression levels of CXCR6 mRNA in normal epidermal cell lines (HACAT) and HNSCC cell lines (SCC9, SCC25) (n=3). (g): Immunohistochemical results of CXCR6 in tumor tissues and adjacent normal tissues of HNSCC patients from our central hospital (20×). Scale bar = 100 μm. The data were expressed as mean±SEM, n=3. M: distant metastasis; N: lymph node metastasis; ns: no significant; ***P < 0.001; CXCL16: CXC motif chemokine ligand 16; HNSCC: head and neck squamous carcinoma; mRNA: messenger RNA; TCGA: The Cancer Genome Atlas; CXCR6: CXC chemokine receptor 6; SEM: standard error of mean.

Fig. S2 Validation of mRNA levels of unregulated genes in the transcriptome results (n=3). The data were expressed as mean±SEM, n=3. ***P < 0.001; **P < 0.01; *P < 0.05. RPL27A: ribosomal Protein L27A; SEM: standard error of mean.

Fig. S3 Results of clone formation experiments of SCC9 and SCC25 cells after the combination of ED-71 and si-CXCL16. (a): ED-71 and si-CXCL16 inhibited the clone formation of SCC9 cells after co-action. (b): ED-71 and si-CXCL16 inhibited the clone formation of SCC25 cells after co-action.

unedited